

# Natural convection from a spinning cone in Casson fluid embedded in porous medium with injection, temperature dependent viscosity and thermal conductivity

GILBERT MAKANDA  
 Central University of Technology  
 Department of Mathematical  
 and Physical Sciences  
 Free State, Private Bag X20539,  
 Bloemfontein, 9300  
 SOUTH AFRICA  
 gilbertmakanda@yahoo.com

PRECIOUS SIBANDA  
 School of Mathematics, Statistics  
 and Computer Science,  
 University of Kwa-Zulu Natal  
 Private bag, X01, Scottsville 3209,  
 Pietermaritzburg  
 SOUTH AFRICA  
 sibandap@ukzn.ac.za

*Abstract:* In the present study, a numerical analysis on natural convection Casson fluid flow from a spinning cone in porous medium with injection, temperature-dependent viscosity and thermal conductivity is considered. The surface of the cone is heated under linear surface temperature (LST). The boundary layer partial differential equations were converted into a system of ordinary differential equations which were then solved using spectral relaxation method (SRM). In this study, we study the effects of varying fluid parameters on logarithm of the SRM decoupling error. The results obtained in this study were compared with others in the literature and found to be in excellent agreement. The application of the SRM on a spinning cone has not been studied. The boundary layer velocity, temperature and concentration profiles are computed for different values of the physical parameters. In particular, the effect of the Casson parameter, spin parameter, Eckert number, temperature dependent viscosity parameter, thermal conductivity parameter on rotational velocity and temperature profiles was studied. Increasing the Casson and temperature-dependent viscosity parameters both reduce the logarithm of the SRM decoupling error. Increasing the Eckert and spin parameters both increase the logarithm of the SRM decoupling error.

*Key-Words:* Casson fluid, spinning cone, partial slip, Spectral relaxation method

## 1 Introduction

The problem of free convection from spinning objects has attracted attention from researchers due to their practical application in industry. The applications of natural convection from spinning objects in conjunction to temperature dependent viscosity and thermal conductivity arise in molten metals, manufacturing of plastics, paints, design of cooking materials.

Studies in free or natural convection have been done by several researchers among others Chamkha and Rashad [2], who studied natural convection from a vertical cone in a nanofluid in porous media. Narayana et al. [3] investigated free magnetohydrodynamic flow and convection from a spinning cone. Ece [4] studied free convection flow about a cone under mixed thermal boundary conditions in the presence of a magnetic field. Other studies on cone geometry include those of Cheng [5], [6] and [7] who explored free convection fluid flow under variable temperature, mixed boundary conditions in porous media and Soret and Dufour effects.

Agarwal and Rakich [8] studied hypersonic laminar viscous flow past spinning cones at angle of attack. Anilkumar and Roy [9] studied mixed convection flow on a rotating cone in a rotating fluid. Dinarvand et al. [10] investigated micropolar fluid flow and heat trans-

fer about a spinning cone with Hall current and Ohmic heating. Datta [11] studied boundary layer flow of the Reiner Rivlin fluid near a spinning cone. Other studies on cones include those of Takhar [12], Saleh [13], Alim et al. [14], Narayana et al. [15] and Awad et al. [16].

The study of Casson fluid flow has been done by many researchers, examples of these fluids are toothpaste, soup, blood, paint etc. Ramachandra et al. [17] investigated the flow of Casson fluid from a horizontal cylinder with partial slip. Mukhophadyay and Vajravelu [18] studied diffusion of chemically reactive species in Casson fluid flow. The study of Casson fluid flow were also done by among others Mukhophadyay et al. [19], Nadeem et al. [20], Pramanic [21] and Hayat et al. [22]. These studies advanced the research in Casson fluid flow, they studied Casson fluid flow over unsteady and exponentially stretching surfaces stretching surfaces in the presence of thermal radiation and porous medium.

The study of Casson fluid flow is more practical when temperature-dependent viscosity and thermal conductivity on the surface of flow is considered. The consideration of these aspects have been done by among others Animasaun [23], who considered variable viscosity and thermal conductivity along an exponentially stretching sheet embedded in a thermally

stratified medium with exponentially heat generation. Animasaun [24] further considered Casson fluid flow with variable therm-physical property. Miyauchi and Kameyama [25] studied influences of the depth dependence of thermal conductivity on thermal convection with temperature dependent viscosity. Aziz and Khan [26] considered thermal conductivity and temperature dependent viscosity in their study. Jha et al. [27] investigated natural convection flow in vertical annular microchannel having temperature dependent viscosity. Costa and Macedonio [28] considered viscous heating in fluids temperature-dependent viscosity with implications on magma flows. Rundora and Makinde [29] also investigated effects of Navier slip on unsteady flow of a reactive variable viscosity in a non-Newtonian fluid.

In the present study we investigate the effects of temperature-dependent viscosity and thermal conductivity in natural convection from a spinning cone with injection in porous medium. The present work is also a further development of the work of Makanda and Sibanda [1] in which the linear surface temperature (LST) and linear surface heat flux (LSHF) are considered. The study of Casson fluid has not been widely investigated for heat transfer past a spinning cone. Similarity transformations are used to convert the governing equations into a system of ordinary differential equations which are then solved by using the spectral relaxation method (SRM). The numerical method used is validated by comparison to previous work by other authors. In this work we investigate the effect of varying physical parameters on the convergence of the numerical method used. We further study the effects of various fluid parameters on velocity  $f'(\eta)$ , rotational velocity  $g(\eta)$  and temperature  $\theta(\eta)$  profiles with the presentation of graphical illustrations.

## 2 Mathematical formulation

The steady, laminar, viscous and buoyancy driven convection heat transfer flow from a spinning vertical cone with injection, temperature-dependent viscosity and thermal conductivity effects in a Casson fluid. The surface of the cone maintained at a uniform temperature  $T_a (> T_\infty)$ .  $\Omega$  is the angular velocity of the spinning cone,  $u, v$  and  $w$  are the velocity components in the  $x, y$  and  $z$  respectively.  $g$  is the acceleration due to gravity (see Figure 1).

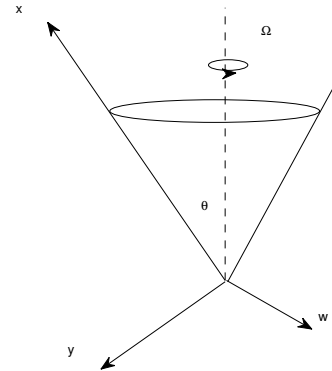


Figure 1: Schematic diagram of the spinning cone

The rheological equation of state for an isotropic and incompressible flow of a Casson fluid is given as

$$\tau_{ij} = \left( \mu_e^{\frac{1}{n}} + (\tau_y / \sqrt{2\pi})^{\frac{1}{n}} \right)^n e_{ij}, \quad |\tau_{ij}| > \tau_y(1)$$

if  $|\tau_{ij}| < \tau_y$  then  $\pi = 0$ , there is no flow

where  $\mu_e$  is plastic dynamic viscosity of the Casson fluid,  $\tau_y$  is the yield stress of fluid,  $\pi$  is the product of the component of deformation rate with itself, namely,  $\pi = e_{ij}e_{ij}$ ,  $e_{ij}$  is the  $(i, j)$ -th component of the deformation rate. For  $n = 2$  we have the simple model for Casson fluid. In this paper we adopt the value  $n = 1$  as used in [18],[19],[17]. The governing equations in this flow are given as;

$$\frac{\partial}{\partial x}(ru) + \frac{\partial}{\partial y}(rv) = 0, \tag{2}$$

$$u \frac{\partial u}{\partial x} + v \frac{\partial u}{\partial y} - \frac{w^2}{x} = \frac{\mu(T)}{\rho} \left( 1 + \frac{1}{\beta} \right) \frac{\partial^2 u}{\partial y^2} - \frac{\mu(T)}{\rho K} u + \frac{1}{\rho} \frac{\partial \mu(T)}{\partial T} \frac{\partial T}{\partial y} \frac{\partial u}{\partial y} + g\beta_T(T - T_\infty) \cos \theta, \tag{3}$$

$$u \frac{\partial w}{\partial x} + v \frac{\partial w}{\partial y} + \frac{uw}{x} = \frac{\mu(T)}{\rho} \left( 1 + \frac{1}{\beta} \right) \frac{\partial^2 w}{\partial y^2} - \frac{\mu(T)}{\rho} \frac{w}{K}, \tag{4}$$

$$u \frac{\partial T}{\partial x} + v \frac{\partial T}{\partial y} = \frac{k(T)}{\rho C_p} \frac{\partial^2 T}{\partial y^2} + \frac{1}{\rho C_p} \frac{\partial k(T)}{\partial T} \left( \frac{\partial T}{\partial y} \right)^2 + \frac{\mu(T)}{\rho C_p} \left( 1 + \frac{1}{\beta} \right) \left( \frac{\partial u}{\partial y} \right)^2 \tag{5}$$

Eqs. (2)-(5) are subject to boundary conditions

$$\begin{aligned} u &= 0, v = -V_a, w = r\Omega, \\ T &= T_\infty + A\left(\frac{x}{L}\right), y = 0, \\ u &\rightarrow 0, w \rightarrow 0, T \rightarrow T_\infty, \text{ as } y \rightarrow \infty, \end{aligned} \tag{6}$$

where the subscripts  $a$  and  $\infty$  refer to the surface and ambient conditions.

We assume linear surface temperature on the cone surface. The dynamic viscosity and thermal conductivity varies as a linear function of temperature as in Animasaun [23].

$$\begin{aligned} \mu(T) &= \mu_0[a_1 + b_1(T_a - T)] \\ \kappa(T) &= \kappa_0[a_2 + b_2(T - T_\infty)] \end{aligned} \tag{8}$$

where  $\mu_0$  is the coefficient of viscosity and  $\kappa_0$  is the constant value of the coefficient of thermal conductivity further away from the cone surface,  $\rho$  is the density of the fluid.  $A, a_1, a_2, b_1, b_2$  are constants; in this study we consider  $a_1 = a_2 = 1$  only,  $K$  is permeability parameter and  $C_p$  is the specific heat capacity.

We introduce the non-dimensional variables

$$\left. \begin{aligned} (X, Y, R) &= \left(\frac{x}{L}, \frac{y}{L}Gr^{\frac{1}{4}}, \frac{r}{L}\right) \\ (U, V, W) &= \left(\frac{u}{U_0}, \frac{Gr^{\frac{1}{4}}v}{U_0}, r\Omega\right) \\ \bar{T} &= \frac{T - T_\infty}{T_a - T_\infty}, \end{aligned} \right\} \tag{9}$$

where  $U_0 = [g\beta_T(T_a - T_\infty) \cos \phi L]^{\frac{1}{2}}$  The dimensionless groups for this model is given by

$$\left. \begin{aligned} Da &= \frac{K}{L^2}, Gr = \left(\frac{U_0 L}{\nu}\right)^2, Pr^* = \frac{\nu_0}{\alpha}, \\ Ec &= \frac{U_0^2}{C_p(T_w - T_\infty)}, Re = \frac{\Omega L^2}{\nu_0}, \\ \epsilon_1 &= b_1(T_a - T_\infty), \epsilon_2 = b_2(T_a - T_\infty), \end{aligned} \right\} \tag{10}$$

We introduce the stream function  $\psi$  and similarity variables as

$$\left. \begin{aligned} U &= \frac{1}{R} \frac{\partial \psi}{\partial Y}, V = -\frac{1}{R} \frac{\partial \psi}{\partial X}, W = XRg \\ \psi &= XRf(\eta), \bar{T} = X\theta(\eta), \end{aligned} \right\} \tag{11}$$

By first substituting the non-dimensional variables (9) into Eqs. (2)-(5) and using similarity variables (11), the governing equations reduce to

$$\begin{aligned} [1 + \epsilon_1 - \epsilon_1\theta] \left(1 + \frac{1}{\beta}\right) f''' + 2ff'' - f'^2 - \xi g^2 \\ - \epsilon_1\theta'f'' + k_p[1 + \epsilon_1 - \epsilon_1\theta]f' + \theta = 0, \end{aligned} \tag{12}$$

$$\begin{aligned} [1 + \epsilon_1 - \epsilon_1\theta] \left(1 + \frac{1}{\beta}\right) g'' + 2fg' - 2f'g \\ + k_p[1 + \epsilon_1 - \epsilon_1\theta]g = 0, \end{aligned} \tag{13}$$

$$\begin{aligned} (1 + \epsilon_2)\theta'' + Pr(2f\theta' - f'\theta) + \epsilon_2(\theta')^2 \\ + EcPr \left(1 + \frac{1}{\beta}\right) [1 + \epsilon_1 - \epsilon_1\theta]f''^2 = 0 \end{aligned} \tag{14}$$

with boundary conditions;

$$\begin{aligned} f(0) = f_w, f'(0) = 0, g(0) = 1, \theta(0) = 1, \\ f'(\infty) \rightarrow 0, g(\infty) \rightarrow 0, \theta(\infty) \rightarrow 0. \end{aligned} \tag{15}$$

where  $f_w$  is the injection parameter,  $Pr$  is the Prandtl number,  $Da$  is the Darcy number,  $Gr$  is the Grashof number and  $Ec$  is the Eckert number,  $Re$  is the Reynolds number,  $\xi$  is the spin parameter,  $k_p$  is the inertia parameter,  $\epsilon_1$  is the temperature-dependent viscosity parameter and  $\epsilon_2$  is the thermal-conductivity parameter. The parameter  $f_w$  is the blowing/suction parameter. The case  $f_w < 0$  represents blowing and  $f_w > 0$  represents suction. The engineering parameters of interest are the local skin friction coefficient and the local Nusselt number which are defined as follows.

The shear stress at the surface of the cone is given by

$$\tau_a = \frac{\mu \left(1 + \frac{1}{\beta}\right) U_0}{LGr^{-\frac{1}{4}}} Xf''(0) \tag{16}$$

where  $\mu$  is the coefficient of viscosity, the skin friction coefficient is given by

$$C_f = \frac{\tau_a}{\frac{1}{2}\rho U_0^2} \tag{17}$$

Using Eqs.(16) and (17) gives

$$C_f Gr^{\frac{1}{4}} = 2\left(1 + \frac{1}{\beta}\right) Xf''(0). \tag{18}$$

The heat transfer from the cone surface into the fluid is given by

$$q_a = \frac{-k(T_a - T_\infty)}{LGr^{-\frac{1}{4}}} X\theta'(0), \tag{19}$$

$k$  is the thermal conductivity of the fluid, The Nusselt number under LST is given by

$$Nu = \frac{L}{k} \frac{q_a}{T_a - T_\infty} \tag{20}$$

Eqs.(19) and (20) together with Eqs. (9) and (10) give

$$NuGr^{-\frac{1}{4}} = -X\theta'(0). \tag{21}$$

### 3 Results and discussion

In this section we discuss the physics of the problem by studying the effects of the physical parameters on velocity  $f'(\eta)$ , rotational velocity  $g(\eta)$  and temperature profiles  $\theta(\eta)$ . We also study the variation of both skin friction and local Nusselt number with the physical parameters. For validation of the numerical method used in this study, results for the skin friction coefficient  $f''(0)$  and heat transfer coefficient  $-\theta'(0)$  for the Newtonian fluid were compared to those of Ece [4] and the SRM, for  $1/\beta \rightarrow 0, \epsilon_1 = \epsilon_2 = f_w = \xi = Ec = 0$  and the Darcian drag force terms  $-k_p f' = k_p g = 0$ . The comparison is shown in Table 1 and it is found to be in excellent agreement to five decimal places.

Table 1: Comparison of the values of  $f''(0)$  and  $-\theta'(0)$  of Ece [4] with the SRM.

Pr	Ece [4]		SRM	
	$f''(0)$	$-\theta'(0)$	$f''(0)$	$-\theta'(0)$
1	0.68150212	0.63886614	0.68148625	0.63885897
10	0.43327726	1.27552680	0.43327848	1.27552816

Table 2: variation of the values of  $\xi$  on  $(1 + \frac{1}{\beta})f''(0)$  and  $-\theta'(0)$  and number of iterations

Pr	$\beta$	$\epsilon_1$	$\epsilon_2$	$\xi$	iter	$(1 + \frac{1}{\beta})f''(0)$	$-\theta'(0)$
1	0	0	0	0	100	0.6814350	0.63885452
1	0	0	0	0.5	100	0.50313924	0.59904833
1	0	0	0	0.9	100	0.34600459	0.55931154

Table 2 shows the effect the variation of the spin parameter  $\xi$  on the skin friction and heat transfer coefficients. Increasing the spin parameter decrease both skin friction and heat transfer coefficients. The different solutions were obtained using in the same number of iterations.

Table 3: variation of the values of  $\beta$  on  $(1 + \frac{1}{\beta})f''(0)$  and  $-\theta'(0)$  and number of iterations

Pr	$\beta$	$\epsilon_1$	$\epsilon_2$	$\xi$	iter	$(1 + \frac{1}{\beta})f''(0)$	$-\theta'(0)$
1	1	0	0	0	68	0.3997800	0.56724300
1	3	0	0	0	91	0.5419735	0.60638362
1	5	0	0	0	95	0.58667938	0.61667938

Table 3 shows the effect the variation of the Casson parameter  $\beta$  on the skin friction and heat transfer coefficients. Increasing the Casson parameter increase both skin friction and heat transfer coefficients. Increasing the Casson parameter increased number of iterations at which the solutions were obtained.

Table 4: variation of the values of  $\epsilon_1$  on  $(1 + \frac{1}{\beta})f''(0)$  and  $-\theta'(0)$  and number of iterations

Pr	$\beta$	$\epsilon_1$	$\epsilon_2$	$\xi$	iter	$(1 + \frac{1}{\beta})f''(0)$	$-\theta'(0)$
1	0	0	0	0	100	0.67170865	0.63618631
1	0	0.2	0	0	100	0.67394360	0.63303648
1	0	0.4	0	0	97	0.67618974	0.63002538

Table 4 shows the effect the variation of the temperature-dependent viscosity parameter  $\epsilon_1$  on the skin friction and heat transfer coefficients. Increasing the temperature-dependent viscosity parameter increase skin friction and decrease heat transfer coefficients. The different solutions were obtained using different number of iterations.

Table 5: variation of the values of  $\epsilon_2$  on  $(1 + \frac{1}{\beta})f''(0)$  and  $-\theta'(0)$  and number of iterations

Pr	$\beta$	$\epsilon_1$	$\epsilon_2$	$\xi$	iter	$(1 + \frac{1}{\beta})f''(0)$	$-\theta'(0)$
1	0	0	0	0	100	0.66450388	0.63755644
1	0	0	0.2	0	100	0.68083002	0.63458268
1	0	0	0.4	0	100	0.69589002	0.63060665

Table 5 shows the effect the variation of the thermal conductivity parameter  $\epsilon_2$  on the skin friction and heat transfer coefficients. Increasing the thermal conductivity parameter increase skin friction and decrease heat transfer coefficients. The different solutions were obtained using the same number of iterations.

Table 6: variation of the values of  $Pr$  on  $(1 + \frac{1}{\beta})f''(0)$  and  $-\theta'(0)$  and number of iterations

Pr	$\beta$	$\epsilon_1$	$\epsilon_2$	$\xi$	iter	$(1 + \frac{1}{\beta})f''(0)$	$-\theta'(0)$
0.7	0	0	0	0	100	0.73015561	0.53907580
1	0	0	0	0	100	0.67282338	0.63459328
5	0	0	0	0	38	0.38363922	1.70342833

Table 6 shows the effect the variation of the Prandtl number  $Pr$  on the skin friction and heat transfer coefficients. Increasing the Prandtl number decrease skin friction coefficient and increase heat transfer coefficient. The different solutions were obtained in different number of iterations.

The problem of free convection Casson fluid flow from a spinning cone in porous medium with injection, temperature-dependnt viscosity and thermal conductivity is solved numerically using the spectral relaxation method (SRM). The results depicted in Figures 2-16 are the results obtained by SRM. A tolerance of  $10^{-8}$  for the method was used. The values are generated at selected values of the Darcian-drag force term  $k_p$ , the Prandtl number  $Pr$ , and the Casson parameter  $\beta$ .

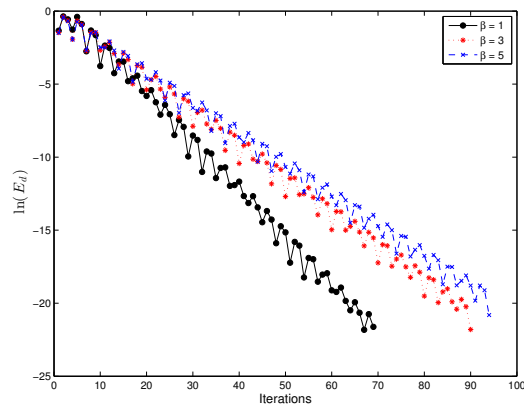


Figure 2: Effects of varying  $\beta$  on logarithm of SRM on decoupling error

Figure 2 shows the effect of increasing the Casson parameter on convergence of the method used. Increasing the Casson parameter result in the increased error (non-accurate) at the same number of iterations. Increasing the Casson parameter would have an effect on the condition number of the solution matrix of the system of equations making it less accurate. The case  $\beta = 1$  yields the solution in only 70 iterations compared to the other two cases  $\beta = 3, 5$  that yields the soultion after more than 90 iterations.

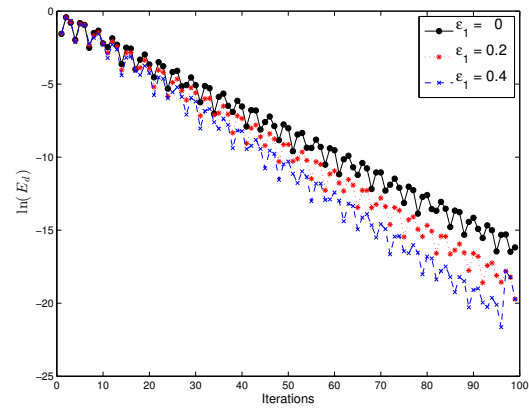


Figure 4: Effects of varying  $\epsilon_1$  on logarithm of SRM on decoupling error

Figure 4 shows the effect of increasing the temperature-dependent viscosity parameter on convergence of the method used. Increasing the temperature-dependent viscosity parameter result in the reduction of the error at the same number of iterations. Increasing this parameter affects the system matrix condition number in way that increase the accuracy of the solution. The case  $\epsilon_1 = 0$  is less accurate than the other two cases.

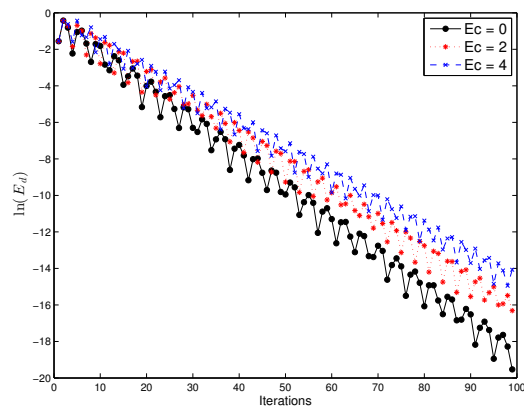


Figure 3: Effects of varying  $Ec$  on logarithm of SRM on decoupling error

Figure 3 shows the effect of increasing the Eckert number on convergence of the method used. Increasing the Eckert number result in the increase in error at the same number of iterations. Increasing the Eckert number would affect the matrix condition number in the same manner as the Casson parameter but the case  $Ec = 0$  yields more accurate solutions than than the cases  $Ec = 2, 4$  after the same number of iterations.

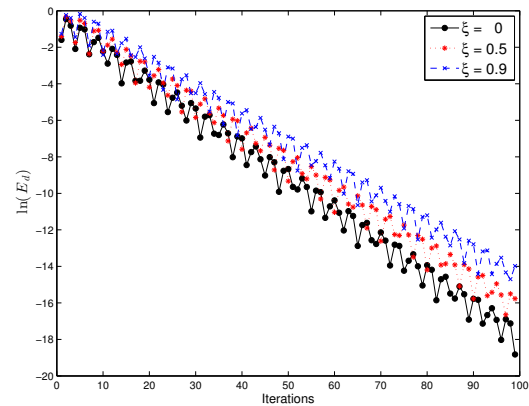


Figure 5: Effects of varying  $\xi$  on logarithm of SRM on decoupling error

Figure 5 shows the effect of increasing the spin parameter on convergence of the method used. Increasing the spin parameter result in the increase in error at the same number of iterations. This parameter affects the condition number in such a way that it reduces the accuracy of the method. The case  $\xi = 0$  yields more accurate solutions than the other two cases.

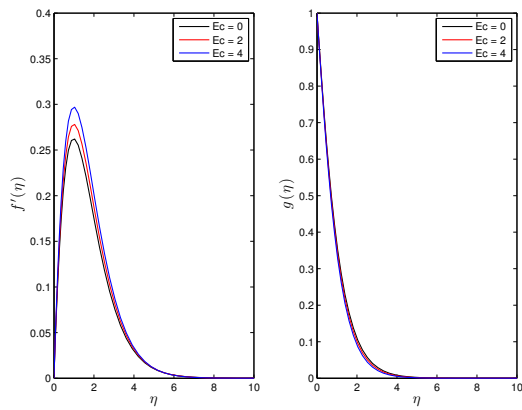


Figure 6: Effects of varying  $Ec$  on rotational velocity and velocity profiles

Figure 6 depict the effect of increasing the Eckert number  $Ec$  on velocity  $f'(\eta)$  and rotational velocity  $g(\eta)$  profiles. Increasing the Eckert number increase  $f'(\eta)$  profiles and decrease rotational  $g(\eta)$  velocity profiles. Increasing the Eckert number increase temperature in the boundary layer thereby increasing velocity close to the boundary. The rotational velocity is decreased due to the increase  $f'(\eta)$  which is in the perpendicular direction to the rotational velocity  $g(\eta)$ .

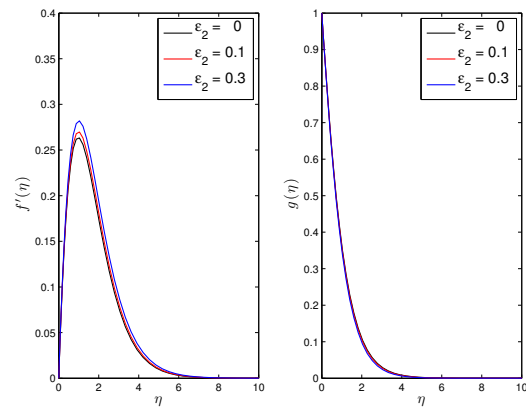


Figure 8: Effects of varying  $\epsilon_2$  on rotational velocity and velocity profiles

Figure 8 show the effect of increasing the thermal conductivity parameter  $\epsilon_2$  on velocity  $f'(\eta)$  and rotational velocity  $g(\eta)$  profiles. Increasing the thermal conductivity parameter increase  $f'(\eta)$  profiles and decrease rotational  $g(\eta)$  velocity profiles. Increasing the thermal conductivity increase the surface temperature causing an increase in the velocity profiles. The reduction in rotational velocity is due to the fact that rotation is perpendicular direction to the velocity profiles.

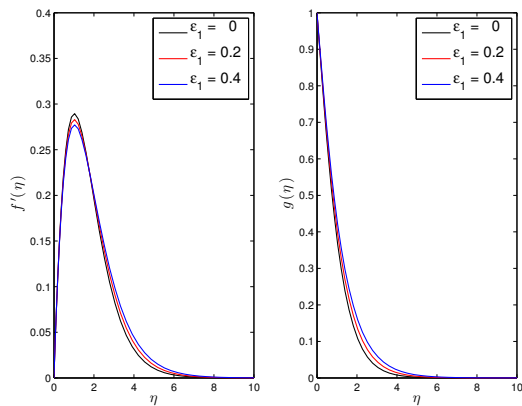


Figure 7: Effects of varying  $\epsilon_1$  on rotational velocity and velocity profiles

Figure 7 show the effect of increasing the temperature-dependent viscoisty parameter  $\epsilon_1$  on velocity  $f'(\eta)$  and rotational velocity  $g(\eta)$  profiles. Increasing the temperature-dependent viscoisty parameter increase both  $f'(\eta)$  profiles and rotational  $g(\eta)$  velocity profiles. Increasing the temperature-dependent viscosity would have an effect of increasing the velocity profiles close to the cone surface caused by higher temperatures. A reverse effect is noted further from the surface due to lower temperatures and high viscosity. The rotational velocity increases is more pronounced at the surface due to the spinning cone.

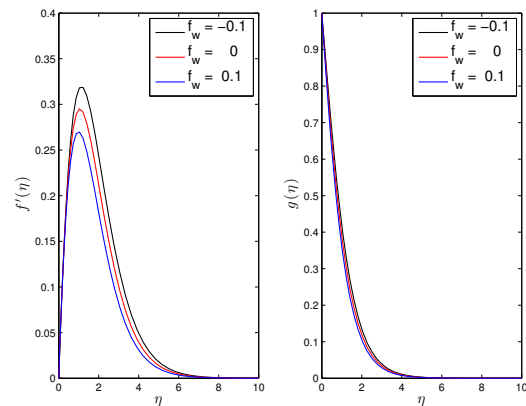


Figure 9: Effects of varying  $f_w$  on rotational velocity and velocity profiles

Figure 9 show the effect of increasing the injection parameter  $f_w$  on velocity  $f'(\eta)$  and rotational velocity  $g(\eta)$  profiles. Increasing the injection parameter increase both velocity  $f'(\eta)$  profiles and rotational  $g(\eta)$  velocity profiles. Injection of more fluid at the surface of the cone tend to assist the flow. As more fluid is introduced into the boundary layer, rotation sweeps it across the cone and this fluid mass tend to assist rotational velocity due to inertia.

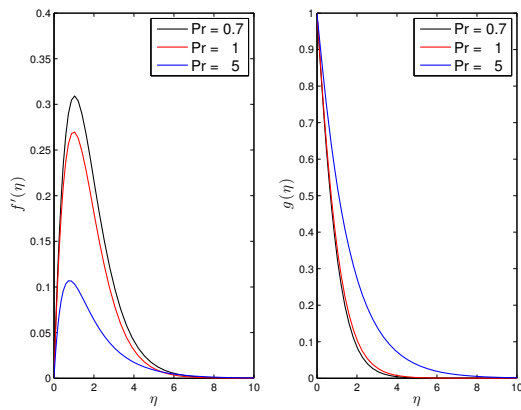


Figure 10: Effects of varying  $Pr$  on rotational velocity and velocity profiles

Figure 10 show the effect of increasing the Prandtl number  $Pr$  on velocity  $f'(\eta)$  and rotational velocity  $g(\eta)$  profiles. Increasing the Prandtl number decrease the  $f'(\eta)$  profiles and increase rotational  $g(\eta)$  velocity profiles. Increased Prandtl numbers mean smaller thermal boundary layer than the momentum boundary layer. There is low temperature which reduce velocity profiles. Rotational velocity profiles are increased to a larger momentum boundary layer.

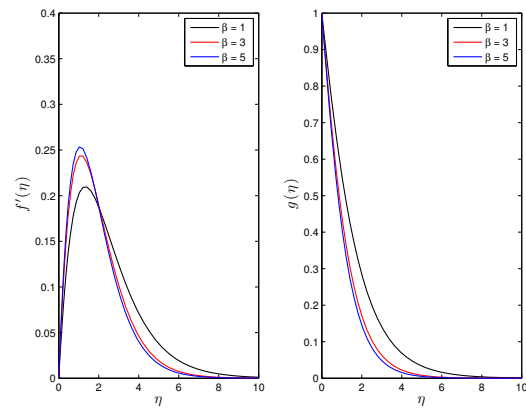


Figure 12: Effects of varying  $\beta$  on rotational velocity and velocity profiles

Figure 12 show the effect of increasing the Casson parameter  $\beta$  on velocity  $f'(\eta)$  and rotational velocity  $g(\eta)$  profiles. Increasing the Casson parameter decrease both the  $f'(\eta)$  profiles and rotational  $g(\eta)$  velocity profiles. Increasing the Casson parameter tend to make the fluid more Newtonian increasing the velocity profiles close to the surface, the reverse effect noted is due to rotation. The increase in velocity profiles noted close to the surface cause a reduction in the rotational velocity.

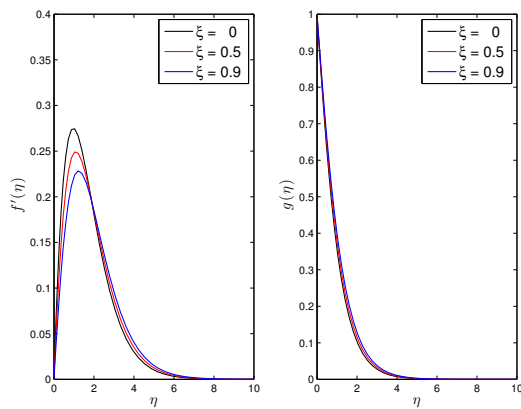


Figure 11: Effects of varying  $\xi$  on rotational velocity and velocity profiles

Figure 11 show the effect of increasing the spin parameter  $\xi$  on velocity  $f'(\eta)$  and rotational velocity  $g(\eta)$  profiles. Increasing the spin parameter decrease the  $f'(\eta)$  profiles and increase rotational  $g(\eta)$  velocity profiles. Increasing the spin parameter tends to assist rotation but reduce the velocity profiles to the direction of the spin which acts perpendicular to the velocity profiles.

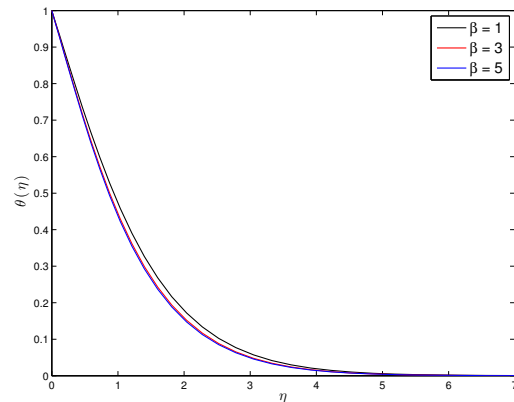


Figure 13: Effects of Casson parameter  $\beta$  on temperature profiles

Figure 13 show the effect of increasing the Casson parameter  $\beta$  on temperature  $\theta(\eta)$  profiles. Increasing the Casson parameter decrease temperature profiles. Increasing the Casson parameter implies less velocity due to low temperature in the boundary layer thereby reducing temperature profiles.

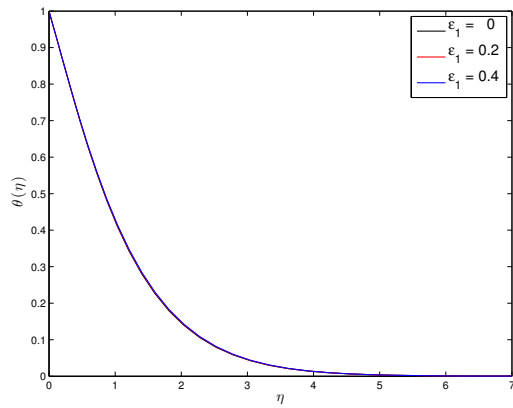


Figure 14: Effects of temperature-dependent viscosity  $\epsilon_1$  on temperature profiles

Figure 14 show the effect of increasing the temperature-dependent viscosity  $\epsilon_1$  on temperature  $\theta(\eta)$  profiles. Increasing the temperature-dependent viscosity decrease temperature profiles. The temperature and viscosity are inversely proportional. If the temperature increase the viscoisty reduces. Therefore increasing the viscosity parameter would have an effect of decreasing the temperature.

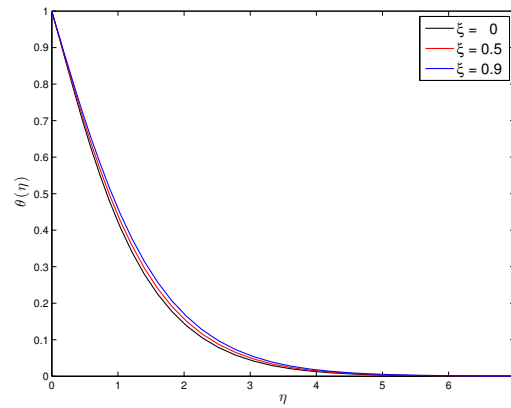


Figure 16: Effects of spin parameter  $\xi$  on temperature profiles

Figure 15 show the effect of increasing the spin parameter  $\xi$  on temperature  $\theta(\eta)$  profiles. Increasing the spin parameter increase temperature profiles. As the spin parameter is increased there is more molecule interaction in the boundary layer causing a rise in temperature sometimes referred to as viscous dissipation.

### 4 Conclusion

The investigation presented in this analysis of effects of temperature-dependent viscosity and thermal conductivity on free convection from a spinning cone with injection in Casson fluid in porous medium provides numerical solutions for the boundary velocity, rotational velocity and heat transfer. The coupled nonlinear governing differential equations were solved using the spectral relaxation method (SRM). The interesting results in this work are the consideration of rotational velocity profiles rarely reported in the literature and the effect of various fluid parameters on the convergence of the numerical method used. It is generally observed that increasing the Casson parameter  $\beta$  and temperature-dependent viscosity parameter both reduce the logarithm of the SRM decoupling error. Increasing both the Eckert number and spin parameter increase the logarithm of the SRM decoupling error. The convergence of the spectral relaxation method (SRM) is stable compared to other numerical methods such as the finite difference, this method can be used to solve boundary value problems. Increasing the Eckert number increase the velocity profiles  $f'(\eta)$  and decrease roational velocity  $g(\eta)$  profiles. Increasing both the Prandtl number and spin parameter decrease the velocity profiles  $f'(\eta)$  and increase roational velocity  $g(\eta)$  profiles. This work opens a way in further research on how to deal with computational errors such as interpolation, discretization, truncation errors and badly scaled or ill-conditioned large matrices.

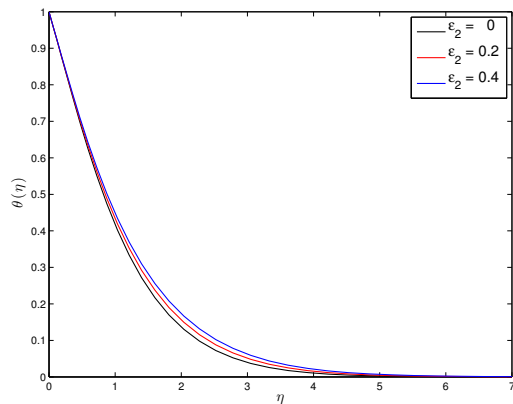


Figure 15: Effects of thermal conductivity parameter  $\epsilon_2$  on temperature profiles

Figure 15 show the effect of increasing the thermal conductivity parameter  $\epsilon_2$  on temperature  $\theta(\eta)$  profiles. Increasing the thermal conductivity parameter increase temperature profiles. Increasing thermal conductivity would have an effect of increasing the surface temperature of the cone thereby increasing temperature in the boundary layer.



## References :

- [1] Makanda G, Sibanda P, Numerical analysis of free convection Casson fluid flow from a spinning cone in non-Darcy porous medium with partial slip and viscous dissipation effects, *International Journal of Mathematical and Computational Methods*, 1 ,(2016), pp. 221-230.
- [2] Chamkha A J, Rashad A. M, Natural convection from a vertical permeable cone in a nanofluid saturated porous media for uniform heat and nanoparticles volume fraction fluxes, *International Journal of Numerical Methods for Heat & Fluid Flow*, 22 ,(2012), pp. 1073-1085.
- [3] Narayana M, Awad F.G, Sibanda P, Free magneto hydrodynamic flow and convection from a vertical spinning cone with cross diffusion effects, *Applied Mathematical Modelling*, 37, (2013), pp. 2662-2678.
- [4] Ece C.M, Free convection flow about a cone under mixed thermal boundary conditions and a magnetic field, *Applied Mathematical Modelling*, 29, (2005), pp. 1121-1134.
- [5] Cheng C.Y, Natural convection boundary layer flow in a micropolar fluid over a vertical permeable cone with variable wall temperature, *International Communications in Heat and Mass Transfer*, 38, (2011), pp. 429-433.
- [6] Cheng C.Y, Natural convection heat transfer of Non-Newtonian fluids in a porous media from a vertical cone under mixed boundary conditions, *International communications in Heat and Mass Transfer*, 36, (2009), pp. 693-697.
- [7] Cheng C.Y, Soret and Dufour's effects on free convection boundary layer over a vertical cylinder in a saturated porous medium, *International communications in Heat and Mass Transfer*, 37, (2010), pp. 796-800.
- [8] Agarwal R, Rakich J. V, Hypersonic laminar viscous flow past spinning cones at angle of attack, *The American Institute of Aeronautics and Astronautics*, 20, (1982), pp. 479-487
- [9] Anilkumar D, Roy S, Unsteady mixed convection flow on a rotating cone in a rotating fluid, *Applied Mathematics and computation*, 155, (2004), pp. 545-561.
- [10] Dinarvand S., Saber M, Abulhasansari M, Micropolar fluid flow and heat transfer about a spinning cone with Hall current and Ohmic heating, *Journal of Mechanical Engineering Science*, doi: 10.1177/0954406213512628
- [11] Datta S. K, The boundary layer flow of the Reiner-Rivlin fluid near a spinning cone, *Applied Scientific Research*, 13, (1964), pp. 194-202.
- [12] Takhar H.S, Rama S.B, Williams R.S, Free convection boundary layer flow of a micropolar fluid past a slender cone, *Mechanics research communications*, 15(3), (1988), pp. 167-176.
- [13] Saleh M.A, A numerical study of natural convection heat transfer with variable viscosity and thermal radiation from a cone and wedge in porous media, *Applied Mathematics and computation*, 170, (2005), pp. 64-75.
- [14] Alim M. A, Alam M, Chowdhury M.K, Pressure work effect on Natural convection flow from a vertical circular cone with suction and non-uniform surface temperature, *Journal of Mechanical Engineering*, ME36, (2006), pp. 6-11.
- [15] Narayana M, Sibanda P, On the solution of double diffusive convective flow due to a cone by a linearization method, *Journal of Applied Mathematics*, doi: 10.1155/2012/587357
- [16] Awad F.G, Sibanda P, and Motsa S.S, Makinde O.D, Convection from an inverted cone in a porous medium with cross diffusion effects, *Computers and mathematics with applications*, 61, (2011), pp. 1431-1441.
- [17] Ramachandra P. V, Subba R.A, Anwa B.O, Flow and heat transfer of Casson fluid from a horizontal cylinder with partial slip in non-Darcy porous medium, *Applied and computational Mathematics*, 2:127, (2013), doi: 10.4172/2168-9679:1000127.
- [18] Mukhopadhyay S, Vajravelu K, Diffusion of chemically reactive species in Casson fluid flow over an unsteady permeable stretching surface, *Journal of Hydrodynamics*, 25, (2013), pp. 591-598.
- [19] Mukhopadhyay S, De P R, Bhattacharyya K, Layek G.C, Casson fluid flow over an unsteady stretching surface, *Ain Shams Engineering Journal*, 4, (2013), pp. 933-938.
- [20] Nadeem S, Ul Haq R, Lee C, MHD flow of a Casson fluid over an exponentially stretching sheet, *Scientia Iranica B*, 19, (2012), pp. 1550-1553.
- [21] Pramanic S, Casson fluid flow and heat transfer past an exponentially porous stretching surface in the presence of thermal radiation, *Ain Shams Engineering journal*, 5, (2014), pp. 205-212 .
- [22] Hayat T, Mustafa M, Pop I, Heat and mass transfer for Soret and Dufour's effect on mixed convection boundary layer flow over a stretching vertical surface in a porous medium filled with viscoelastic fluid, *Commun Nonlinear Sci Numer Simulat*, 15, (2010), pp. 1183-1196.
- [23] Animasaun I. L, Casson Fluid Flow of Variable Viscosity and Thermal Conductivity along Exponentially Stretching Sheet Embedded in a Thermally Stratified Medium with Exponentially Heat Generation, *Journal of Heat and Mass Transfer Research*, 2, (2015), pp. 1-12 .
- [24] Animasaun I. L, E.A. Adebile, A.I. Fagbade, Casson fluid flow with variable thermo-physical property along exponentially stretching sheet

with suction and exponentially decaying internal heat generation using the homotopy analysis method, *Journal of the Nigerian Mathematical Society*, 35, (2016), pp. 1-17.

- [25] Miyauchi A, Kameyama M, Influences of the depth-dependence of thermal conductivity and expansivity on thermal convection with temperature-dependent viscosity, *Physics of the Earth and Planetary Interiors*, 223, (2013), pp. 86-95.
- [26] Aziz A, Khan W. A, Classical and minimum entropy generation analyses for steady state conduction with temperature dependent thermal conductivity and asymmetric thermal boundary conditions: Regular and functionally graded materials, *Energy*, 36, (2011), pp. 6195-6207.
- [27] Jha B. K, Aina B, Rilwanu Z, Steady fully developed natural convection flow in a vertical annular microchannel having temperature dependent viscosity: An exact solution, *Alexandria Engineering Journal*, 55, (2016), pp. 951-958.
- [28] Costa A, Macedonio G, Viscous heating in fluids with temperature-dependent viscosity: implications for magma flows, *Nonlinear Processes in Geophysics*, 10, (2003), pp. 545-555.
- [29] Rundora L, Makinde O. D, Effects of Navier slip on unsteady flow of a reactive variable viscosity non-Newtonian fluid through a porous saturated medium with asymmetric convective boundary conditions, *Journal of Hydrodynamics*, 27, (2015), pp. 934-944.